Crystallization-Induced Energy Level Change of [6,6]-Phenyl-C_{61}-Butyric Acid Methyl Ester (PCBM) Film: Impact of Electronic Polarization Energy

Yufei Zhong[1,2], Seiichiro Izawa[1,2], Kazuhito Hashimoto[1], Keisuke Tajima[2,3], Tomoyuki Koganezawa[4], and Hiroyuki Yoshida[3,5*]*

[1]Department of Applied Chemistry, School of Engineering, The University of Tokyo, 7-3-1 Hongo, Bunkyo-ku, Tokyo 113-8656, Japan

[2]RIKEN Center for Emergent Matter Science (CEMS), 2-1 Hirosawa, Wako 351-0198, Japan

[3]Japan Science and Technology Agency, PRESTO, 4-1-8 Honcho Kawaguchi, Saitama 332-0012, Japan

[4]Japan Synchrotron Radiation Research Institute, 1-1-1 Kouto, Sayo-cho, Sayo-gun, Hyogo 679-5198, Japan

[5]Institute for Chemical Research, Kyoto University, Gokasho, Uji, Kyoto 611-0011, Japan

***Corresponding authors**

Keisuke Tajima:

Hiroyuki Yoshida:

TEL +81-774-38-3083, FAX +81-774-38-3084, E-mail: yoshida@e.kuicr.kyoto-u.ac.jp

Abstract

The effect of thermal annealing on the energy levels of [6,6]-phenyl-C_{61}-butyric acid methyl ester (PCBM) films was investigated using ultraviolet photoelectron spectroscopy, X-ray photoelectron spectroscopy, and low-energy inverse photoemission spectroscopy. We observed that thermal annealing at 150 °C induces reductions in both ionization potential (IP) and electron affinity (EA) with the narrowing of the band gap by 0.1 eV. These changes are associated with crystallization and the reduction in the film thickness by 2.54%. Precise measurements of both IP and EA enabled us to evaluate the effects of the electronic polarization energy in a model based on the charge localized in a single PCBM molecule.

1. Introduction

In high-performance organic solar cells (OSCs), [6,6]-phenyl-C_{61}-butyric acid methyl ester (PCBM) is often used as the electron acceptor in combination with semiconducting polymers and oligomers as donors. The crystallization of materials in OSCs can largely affect device performance by changing mixing morphologies and improve the efficiencies of charge separation, recombination, and collection in organic thin films.[1, 2] The crystallization of donor polymers has generally been considered as the key factor for improving OSC performance owing to improved charge separation and/or transport.[1, 3] Recently, however, the aggregation of PCBM in the films has also been regarded as an important phenomenon for achieving high performance in OSCs. The effect has been discussed in terms of charge delocalization in crystalline domains and the energy level cascade due to the difference in aggregation state.[4, 5]

It is widely accepted that the ionization potential (IP) of the donor and the electron affinity (EA) of the acceptor are key factors to determine the upper limit of open-circuit voltage (V_{OC}) and the efficiency of charge separation. The electronic structures of PCBM films have been investigated by several groups.[6, 7] Yet, how the crystallization of PCBM affects the energy levels has not been clarified, although it has primary importance for photovoltaic processes. Verploegen et al. reported the cold crystallization of PCBM films by thermal annealing at a temperature below the melting point and monitored the effect of blending PCBM with polymers on the crystallization of each component.[8] However, no study on the change in the

electronic structure has been reported.

The energy levels of organic films are affected by many factors such as electronic polarization energy,[9] intermolecular orbital interaction,[10] molecular orientation,[11] surface dipole moment,[12,13] and doping level.[14-16] Namely, the electronic polarization energy originate from the stabilization of charge carriers by the electronic polarization of the surrounding molecules. The magnitude of the electronic polarization energy is about 1 eV,[9] which works to decrease IP and increase EA compared to those of single molecule in vacuum, narrowing the band gap (the difference between IP and EA). The intermolecular orbital interaction discussed here is a quantum chemical effect in condensed phase, broadening of the energy levels up to a few tenth of eV[10] and narrowing of the band gap. The other factors such as molecular orientation, surface dipole, and doping affect both IP and EA equally resulting in a rigid shift of the valence and unoccupied levels without changing the band gap.

Thus far, the above-mentioned effects on the energy levels have been examined using ultraviolet photoemission spectroscopy (UPS) and X-ray photoemission spectroscopy (XPS). With only information about the valence and core levels, it is difficult to distinguish the origin of these effects. Precise determinations of both the band gap and the bandwidth are necessary to distinguish them. Although the bandwidth can be estimated from the peak width of UPS spectrum, no reliable value of the band gap has been available owing to the lack of suitable experimental techniques for the unoccupied states. Inverse photoemission

spectroscopy can be regarded as an inverse process of photoemission and an ideal method of examining unoccupied states. However, the obtained data is not precise enough to discuss changes on the order of 0.1 eV because of the low energy resolution[17] and damage to organic samples due to electron bombardment[18]. If EA can be determined as precisely as IP, it is possible to determine the factors that affect the energy levels.

Recently, we have developed a new experimental method, low-energy inverse photoemission spectroscopy (LEIPS).[19, 20] Electrons with kinetic energy below the damage threshold of organic materials are introduced into the sample film and photons emitted owing to radiative transition to unoccupied states are detected. Since the electron energy is lower than the damage threshold,[21] damage to organic samples is negligible. The energy of emitted photons falls in the range between 2 and 5 eV (i.e., the near-ultraviolet or visible range). These photons can be analyzed using band-pass filters with a high resolution and a high transmittance followed by the use of a highly sensitive photomultiplier. Thus far, this new technique has been applied to small-molecule organic semiconductors[20, 22-24] and polymers[25] to determine EA at a precision higher than 0.1 eV.

In this article, we focus on the change in the energy levels of PCBM films induced by thermal annealing. We find that spin-cast PCBM films thermally annealed above 150 °C crystallize and that their thickness decreases, in association with the change of the energy levels. By determining both IP and EA precisely, we can clearly distinguish the effects of

polarization energy and intermolecular interaction from those of other factors.

2. Experimental Section

PCBM films were prepared by spin coating, typically from $CHCl_3$ solution (10 mg/mL) at 1200 rpm for 60 s, resulting in a film thickness of about 73 nm. Thinner films (approx. 4 nm) were prepared by spin coating from chlorobenzene solution (3 mg/mL) at 3000 rpm for 60 s and used for 2D grazing incidence X-ray diffraction (GIXRD), UPS, XPS, LEIPS, and low-energy electron transmission (LEET) measurements. The substrates were ITO/glass for 2D GIXRD, UPS, XPS, LEIPS, and LEET measurements; SiO_2 (500 nm)/Si for X-ray reflectivity (XRR) measurement; and TiO_2/ITO/glass for GIXRD measurement. Thermal annealing was conducted on a hot plate in a N_2 filled glove box at the designated temperatures for 5 min.

UPS and XPS were performed on a PHI5000 VersaProbe II (ULVAC-PHI Inc.). UPS profiles were obtained with a He (I) excitation energy of 21.2 eV and a pass energy of 5 eV. A bias voltage of −5 V was applied to the samples in order to detect the cutoff region of secondary electrons. XPS profiles were obtained by using Al Kα radiation with a take-off angle of 90°. The XRR and GIXRD measurements were carried out on an X-ray diffractometer (SmartLab, Rigaku, Japan) using monochromatized CuKα radiation (λ = 0.154 nm) generated at 45 kV and 200 mA. GIXRD patterns were measured in the in-plane

geometry at an incident angle of 0.21°. 2D-GIXRD patterns were measured at an incident angle of 0.12° using synchrotron radiation at beamline BL19B2 of SPring-8 with the approval of the Japan Synchrotron Radiation Research Institute.

Details of the LEIPS setup are described elsewhere.[26] The sample specimen was introduced into the vacuum chamber evacuated below 1 x 10^{-7} Pa and incident to an electron beam. To avoid sample damage, the kinetic energy of incident electrons was restricted to less than 4 eV and the electron current densities ranged between 10^{-6} and 10^{-5} A cm^{-2}. Under these experimental conditions, the same IPES profiles were obtained after several scans, confirming that sample damage was negligible. The emitted photons were collected and focused into a photon detector consisting of an optical band-pass filter and a photomultiplier tube. The center wavelengths of the band-pass filters were 254, 280 and 285 nm. The overall energy resolution was estimated to be 0.3 eV. LEET spectroscopy was carried out using the same apparatus and sample films used in LEIPS. The electron current $I(E_k)$ was measured as a function of the electron kinetic energy E_k and the LEET spectrum was obtained as the first derivative $dI(E_k)/dE_k$. The peak corresponds to the VL of the sample.

3. Results

Figure 1a shows the in-plane GIXRD patterns of the PCBM films on the TiO_2/ITO substrate before and after annealing. The film before annealing showed a broad peak at 2θ of

19.7° (d = 0.472 nm calculated from the top of the peak), indicating a disordered structure of PCBM in the film. After annealing the film at 150 °C for 5 min, the broad peak at approximately 19.7° became smaller, a sharp peak at 17.6° (d = 0.539 nm) emerged, and relatively broad peaks appeared at 10.2° and 20.7°. This change suggests the crystallization of PCBM films upon thermal annealing. The annealing temperature was changed from 50 °C to 150 °C, and it was confirmed that the crystallization started occurring above 140 °C (Figure S1a in SI). This crystallization behavior is consistent with the previous report by Verploegen et al.[8] The 2D GIXRD patterns of the films were also measured by using synchrotron radiation. Although only a broad ring was observed in the film before annealing, the diffraction pattern was changed to show a set of clear spots after annealing (Figure S1b and c in SI). This result indicates not only that the film is crystalline after the thermal annealing but also that the domain is preferentially oriented in the film. Although there are several reports on the structural analysis of single-crystal PCBM, we could not identify the structure of the film using known phases.[27, 28] Further detailed study of the crystal structure in PCBM films is needed.

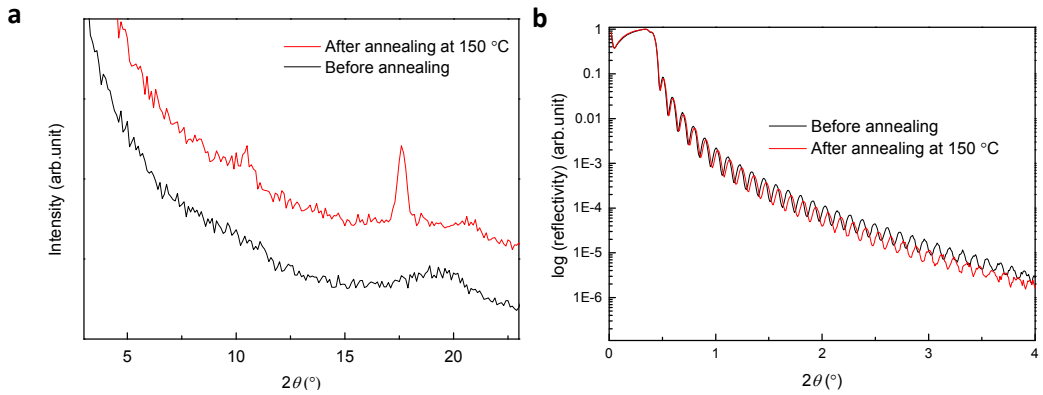

Figure 1. a) In-plane GIXRD and b) XRR patterns of PCBM/TiO_2/ITO sample before and after annealing at 150 °C for 5 min.

The changes in the film thickness and the density before and after annealing were examined using XRR for the PCBM/SiO_2/Si samples. As shown in Figure 1b, both samples showed clear fringes due to the interference of X-rays corresponding to the thickness of the PCBM

layers. Before annealing, the fitting of the data with the bilayer model gave a thickness of 75.24±0.26 nm and a density of 1.644±0.021 g cm^{-3}. After annealing, the fringes shifted to a lower angle and the reflectivity decreased. The fitting of the XRR data gave a thickness of 73.33±0.35 nm and a density of 1.686±0.011 g cm^{-3}. These changes indicate a decrease in PCBM film thickness and an increase in the density upon the crystallization. The thickness is found to be reduced by 2.54±0.60% and the density to be increased by 2.58±1.5%. The change of the density agrees well with that of the thickness, suggesting that the film shrinks along the direction perpendicular to the substrate. Note that XPS measurements of the films confirm the absence of solvent ($CHCl_3$ or chlorobenzene) residue in the films (Figure S2a and b in SI), indicating that the film consists of pure PCBM and is not a co-crystal with the

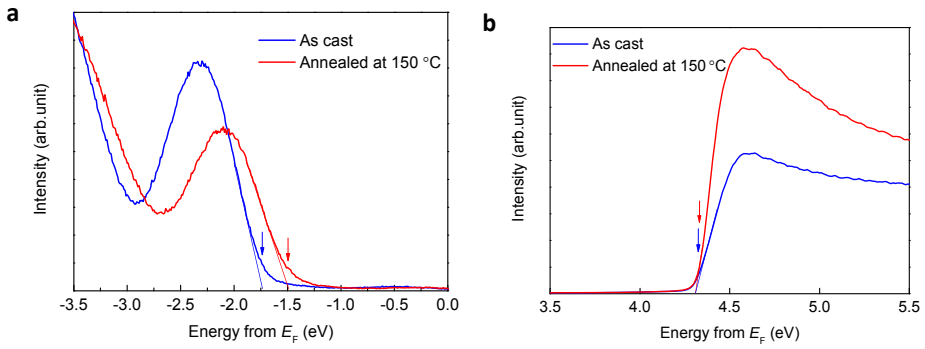

Figure 2. UPS profiles of PCBM films before and after annealing at 150 °C for 5 min in the a) HOMO edge and b) cutoff regions. The arrows indicate the onset energies in panel a) while the cutoff energies in panel b). The abscissa of panel b) is corrected by adding the photon energy (21.2 eV) so that the cut-off energy is expressed as the vacuum level from E_F.

solvent, as in previous report on single-crystal PCBM.[29] This result suggests the increase in film density upon crystallization.

UPS was performed on the samples to monitor the change in the valence energy and vacuum level (VL) of the PCBM films induced by annealing at 150 °C. As shown in Figure 2b, a small difference in the cutoff energy of secondary electrons was found after annealing (4.29 and 4.31 eV before and after annealing, respectively). This indicates little change in VL relative to the Fermi level (E_F) after annealing. In Figure 2a, the onset of the peak in the highest occupied molecular orbital (HOMO) edge region shifted from 1.71 to 1.50 eV after annealing, indicating that the peak consisting of the HOMO of PCBM shifted upward by 0.21 eV relative to E_F. The peak maximum also shifted from 2.32 to 2.07 eV indicating a shift by +0.25 eV. IP was determined as the onset energy of the HOMO peak with respect to the VLs. The IPs were 5.95 and 5.74 eV before and after annealing, respectively. The full width at half-maximum (FWHM) of the HOMO peak was broadened by only 0.03 eV after annealing which was judged from the peak fitted with a Gaussian function. This result suggests a subtle enhancement of the intermolecular orbital coupling of PCBM after annealing, that is, due to the crystallization.

XPS was performed on the films to investigate the energy level change in the core level. Core levels are highly localized and not affected by the change in bandwidth due to intermolecular interaction. The C1s energies before and after annealing were 284.97±0.04 eV and 284.79±0.04 eV, respectively, resulting in an upward shift in the core level by 0.18 eV with respect to E_F (Figure S2c in SI). The decrease in the binding energy is in good agreement with that of IP within experimental uncertainties.

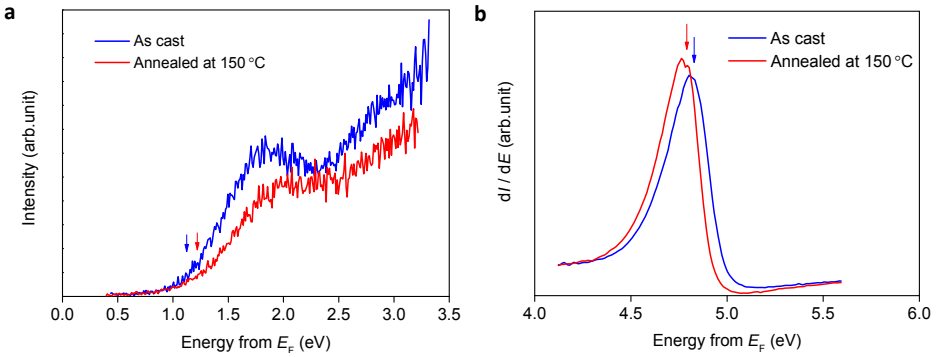

Figure 3. a) LEIPS and b) LEET measurements of PCBM film before and after annealing at 150 °C for 5 min. The arrows indicate a) the onset of the LUMO levels and b) the vacuum levels. The abscissa of panel b) is the energy added by the photon energy so that the peaks correspond to the vacuum levels.

To investigate the change in the EA of PCBM, LEIPS measurements were performed on the films. Figure 3a shows that the onset of the LUMO peak shifts by about 0.1 eV after annealing. LEET measurements of the same films showed that the VLs are 4.80 and 4.76 eV above E_F, respectively (Figure 3b). The change in VL before and after annealing was −0.04

eV. The magnitude of the VL shift is in good agreement with those determined by the cutoff energy of secondary electrons in the UPS measurement, as shown before. This confirms that UPS and LEIPS showed consistent results despite the fact that they were performed using different apparatuses. The absolute VLs determined by secondary electrons of UPS and the peak of LEET differ by a few tenths of an eV. Although VL with respect to E_F may be sensitive to a change in conditions, for example, with exposure to air, the HOMO and LUMO levels are expected to remain unchanged with respect to VL.[30, 31]

To determine EA precisely, LEIPS profiles were measured with different wavelengths of emission, as shown in Figures S3a and b (SI). The extrapolation of the onset in electron

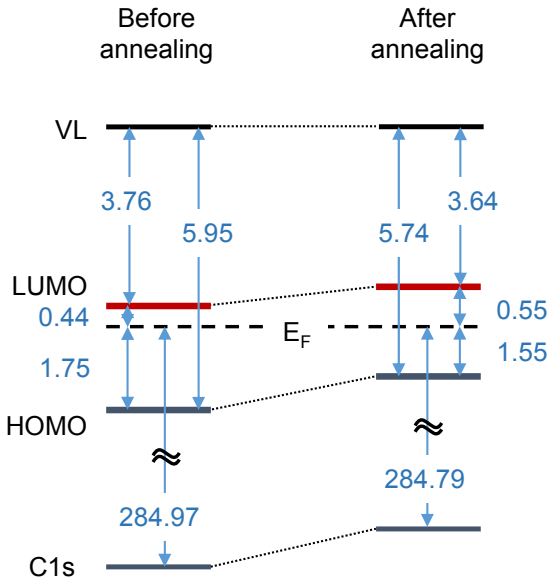

Figure 4. Schematic energy diagrams of PCBM films before and after the crystallization. The unit of the energy is eV. The *y*-axis is relative to the Fermi level but not drawn to scale.

kinetic energy as a function of photon energy gave the EA of the films, as shown in Figure S3c. The EA of PCBM films changed from 3.76 eV to 3.64 eV after annealing, indicating an upward shift of the LUMO band by 0.12±0.01 eV.

The results of UPS, XPS, and LEIPS are summarized as energy diagrams in Figure 4. After the thermal annealing and crystallization of the film, both the LUMO and HOMO levels of PCBM shift upward by 0.12 and 0.21 eV, respectively, relative to VLs. At the same time, the band gap decreases from 2.19 eV to 2.10 eV after annealing.

4. Discussion

The change of the electronic levels can be described by the bandgap narrowing and the rigid shift of the HOMO and LUMO levels as schematically shown in Figure 5. The increase of the electronic polarization energy[9] and the intermolecular orbital interaction[10] narrows the bandgap (Figure 5a) while the molecular orientation,[11] surface dipole moment,[12,13] and doping level[14-16] cause the rigid shift of the energy levels (Figure 5b). We observed that the energy levels of PCBM film show the upward shift by 0.17 eV associated with the reduction of the band bap by 0.09 eV upon the crystallization.

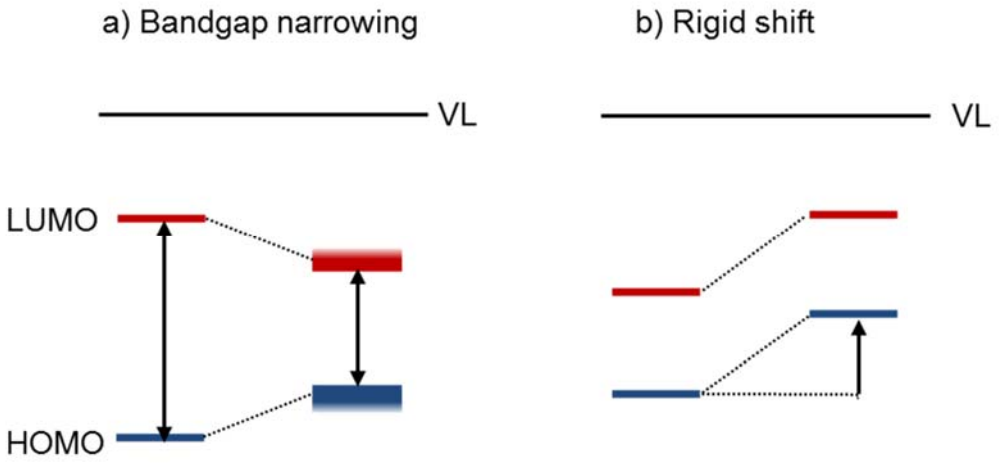

Figure 5. Schematics of energy level changes. a) Bandgap narrowed by the increase of electronic polarizations and broadening of the energy levels. b) Rigid shift of the HOMO and LUMO levels caused by the change of molecular orientation, surface dipole, doping etc.

The electronic polarization energy is the stabilization energy for an ionized species (P_+ and P_- for a cation and an anion, respectively) due to the electronic polarization of the surrounding molecules.[32] An increase in the density of the surrounding media around an ionized molecule should lead to an increase in the electronic polarization energy. In the present study, the XRR results show that the crystallization increases the density of the film; therefore, we expect a larger electronic polarization energy after annealing. Here, we estimate the difference in P_+ and P_- due to the increase in the density of thin films using a simple model.[9] The electrostatic interaction between an ionized molecule and the surrounding molecules is approximated by that between the point charge and the induced dipole. In this

case, P is given by

$$P = 8.25(e)^2 \alpha N^{\frac{4}{3}},$$

where e is the charge of an electron, α is the average molecular polarizability, and N is the number density of molecules. According to this equation, the decrease in the film volume by 3% could induce a 4% increase in P. For PCBM, the reported P_+ and P_- are 1.21 eV and 1.20 eV, respectively. [6, 33] The result shows that the increase in the film density gives rise to a 0.05 eV increase in the electronic polarization energy for both $P+$ and P^-, resulting in a reduction in the band gap by 0.1 eV. Therefore, the P change caused by the densification of the film could quantitatively explain the band gap narrowing.

Another possible cause of band gap narrowing is the enhancement of intermolecular interaction. This should be associated with the broadening of the HOMO and LUMO peaks. However, the observed HOMO peak is broadened only by 0.03 eV (FWHM), which is much smaller than the change in the band gap (0.09 eV). These results suggest that the contribution of changes in the intermolecular orbital coupling is smaller than that of the polarization energy. This conclusion is further supported by the following experimental findings. First, there is virtually no change in the optical gap observed in the photoabsorption spectra of the films (Figure S4 in SI). Second, the change in the C1s peak position (0.18 eV) occurs close to that of the HOMO peak (0.21 eV) suggesting that the effect is predominantly electrostatic rather than the broadening is induced by intermolecular interaction.

In addition to the band gap narrowing, the energy levels shifted upward relative to both VL and E_F after annealing, as shown in Figure 4. Although the reasons for the observed changes are not clear at this moment, we speculated that both molecular orientation and doping level could contribute to the changes. Since the crystallized film shows a preferential orientation as shown by the 2D GIXRD patterns, it is possible that the film surface has a particular molecular orientation after annealing, resulting in the formation of a molecular dipole layer.[11] On the other hand, a small amount of impurities in PCBM could serve as unintentional dopants and be removed, associated with the crystallization by the thermal annealing in N_2. Possible dopants could be oxygen or oxygenated compounds. Bao et al. observed a decrease in the work function of PCBM films by 0.15 eV with exposure to O_2 gas, which was attributed to n-doping.[34] The magnitude of the upward shift of 0.1-0.2 eV in IP and EA observed in the present work is comparable to the reported shift due to oxygen exposure. In our case, the small amount of oxygen included in the PCBM film during the exposure to air might be released upon the annealing. If such de-doping of an n-type dopant is assumed, E_F should shift downward and both HOMO and LUMO bands should shift upward relative to the E_F. [14-16] The change in E_F after the crystallization could compensate for the shifts in the VL, resulting in no apparent change in the VL. According to this picture, the estimated VL shift induced by the crystallization is −0.15 eV. Although change of polarization energy (~0.05 eV) should reduce the band gap and increase EA, the degree of change was smaller than that by

the surface dipole (−0.15 eV). EA therefore, was ultimately decreased by the crystallization.

5. Conclusion

We observed a significant change in the energy levels of PCBM films upon thermal annealing accompanied by the crystallization of the films. From a precise analysis of IP, EA and the core level, we conclude that the band gap narrowing is most likely attributed to the polarization energy due to the increase in film density. The effect of the enhancement of intermolecular interaction upon crystallization could be much smaller. Other factors such as a change in molecular orientation and de-doping may also affect the rigid shift in the HOMO and LUMO levels; in other words, IP and EA change by the same magnitude.

For the calculation of the polarization energy, positive and negative charges are assumed to be point charges. Despite its simplicity, this model could explain the change in the band gap reasonably well, suggesting that charge carriers in PCBM films localized on a single PCBM molecule in the ground state. This picture is consistent with the low mobility of charge carriers in PCBM films.[24]

It is noteworthy that the change in the energy levels should generally occur upon densification. This fact seems to have been overlooked in the discussion of possible cascading energy diagrams in bulk heterojunction structures. The current finding obtained by LEIPS suggests that crystallized, high-density PCBM in OSCs could have significantly

different energy levels from noncrystallized domains through polarization energy changes. This could potentially help to understand the factors that make PCBM the most successful electron acceptor in OSCs.

Acknowledgements: This research was supported by PRESTO, Japan Science and Technology Agency. Y.F.Z. thanks the Chinese Scholarship Council for financial support. The authors thank Dr. Kouki Akaike for fruitful discussions and Ms. Mari Saito (Rigaku) for advice on XRR measurements. GIXRD experiments were performed at the BL19B2 of SPring-8 with the approval of the Japan Synchrotron Radiation Research Institute (JASRI) (Proposal No. 2013B1719).

References

1. T. M. Clarke, A. M. Ballantyne, J. Nelson, D. D. C. Bradley and J. R. Durrant, *Adv. Func. Mater.* 2008, **18**, 4029-4035.
2. T. M. C. a. J. R. Durrant, *Chem. Rev.* 2010, **110**, 6736-6767.
3. G. Li, V. Shrotriya, J. Huang, Y. Yao, T. Moriarty, K. Emery and Y. Yang, *Nat. Mater.* 2005, **4**, 864-868.
4. F. C. Jamieson, E. B. Domingo, T. McCarthy-Ward, M. Heeney, N. Stingelin and J. R. Durrant, *Chem. Sci.* 2012, **3**, 485-492.
5. S. Gelinas, A. Rao, A. Kumar, S. L. Smith, A. W. Chin, J. Clark, T. S. van der Poll, G. C. Bazan and R. H. Friend, *Science* 2014, **343**, 512-516.
6. K. Akaike, K. Kanai, H. Yoshida, J. y. Tsutsumi, T. Nishi, N. Sato, Y. Ouchi and K. Seki, *J. Appl. Phys.* 2008, **104**, 023710.
7. Z.-L. Guan, J. B. Kim, H. Wang, C. Jaye, D. A. Fischer, Y.-L. Loo and A. Kahn, *Org. Electron.* 2010, **11**, 1779-1785.
8. E. Verploegen, R. Mondal, C. J. Bettinger, S. Sok, M. F. Toney and Z. Bao, *Adv. Func. Mater.* 2010, **20**, 3519-3529.
9. N. Sato, K. Seki and H. Inokuchi, *J. Chem. Soc., Faraday Trans.* 1981, **2**, 1621-1633.
10. N. Ueno and S. Kera, *Prog. Surf. Sci.* 2008, **83**, 490-557.
11. S. Duhm, G. Heimel, I. Salzmann, H. Glowatzki, R. L. Johnson, A. Vollmer, J. P. Rabe and N. Koch, *Nat. Mater.* 2008, **7**, 326-332.
12. Q.-S. Wei, K. Tajima, Y. Tong, S. Ye, and K. Hashimoto, *J. Am. Chem. Soc.* 2009, **131**, 17597.
13. Y. Geng, Q. Wei, K. Hashimoto and K. Tajima, *Chem. Mater.* 2011, **23**, 4257.
14. W. Gao and A. Kahn, *Appl. Phys. Lett.* 2001, **79**, 4040.
15. S. Guo, S. B. Kim, S. K. Mohapatra, Y. Qi, T. Sajoto, A. Kahn, S. R. Marder and S. Barlow, *Adv. Mater.* 2012, **24**, 699-703.
16. Y. Qi, S. K. Mohapatra, S. Bok Kim, S. Barlow, S. R. Marder and A. Kahn, *Appl. Phys. Lett.* 2012, **100**, 083305.
17. P. I. Djurovich, E. I. Mayo, S. R. Forrest and M. E. Thompson, *Org. Electron.* 2009, **10**, 515-520.
18. K. Tsutsumi, H. Yoshida and N. Sato, *Chem. Phys. Lett.* 2002, **361**, 367-373.
19. H. Yoshida, *Chem. Phys. Lett.* 2012, **539-540**, 180-185.
20. H. Yoshida, *Anal. Bioanal. Chem.* 2014, **406**, 2231-2237.
21. B. Boudaiffa, P. Cloutier, D. Hunting, M. A. Huels and L. Sanche, *Science* 2000, **287**, 1658-1660.
22. H. Yoshida, *Mater. Res. Soc. Symp. Proc.* 2012, **1493**, 295-301.

23. W. Han, H. Yoshida, N. Ueno and S. Kera, *Appl. Phys. Lett.* 2013, **103**, 123303.
24. Y. Ie, M. Karakawa, S. Jinnai, H. Yoshida, A. Saeki, S. Seki, S. Yamamoto, H. Ohkita and Y. Aso, *Chem. Commun.* 2014, **50**, 4123-4125.
25. S. Fabiano, H. Yoshida, Z. H. Chen, A. Facchetti and M. A. Loi, *ACS Appl. Mater. Interfaces* 2013, **5**, 4417-4422.
26. H. Yoshida, *Rev. Sci. Instrum.* 2014, **85**, 016101.
27. M. Casalegno, S. Zanardi, F. Frigerio, R. Po, C. Carbonera, G. Marra, T. Nicolini, G. Raos and S. V. Meille, *Chem. Commun.* 2013, **49**, 4525-4527.
28. G. Paternò, A. J. Warren, J. Spencer, G. Evans, V. G. Sakai, J. Blumberger and F. Cacialli, *J. Mater. Chem. C* 2013, **1**, 5619-5623.
29. M. T. Rispens, A. Meetsma, R. Rittberger, C. J. Brabec, N. S. Sariciftci and J. C. Hummelen, *Chem. Commun.* 2003, 2116-2118.
30. T. Sueyoshi, H. Kakuta, M. Ono, K. Sakamoto, S. Kera and N. Ueno, *Appl. Phys. Lett.* 2010, **96**, 093303.
31. F. Bussolotti., S. Kera K. Kudo, A. Kahn and N. Ueno, *Phys. Rev. Lett.* 2013, **110,** 267602.
32. F. Gutmann and L. E. Lyons, *Organic Semiconductors,* Chap. 6 (John Wiley and Sons, Inc., 1967).
33. H. Yoshida, *J. Phys. Chem. C* , 2014, **118,** 24377.
34. Q. Bao, X. Liu, S. Braun and M. Fahlman, *Adv. Energy. Mater.* 2013, **4**, 1301272.

Table of Contents Figure